nature communications

Article

https://doi.org/10.1038/s41467-025-61487-6

Intracranial directed connectivity links subregions of the prefrontal cortex to major depression

Received: 7 September 2024

Accepted: 23 June 2025

Published online: 09 July 2025

Check for updates

John Myers[1] ✉, Jiayang Xiao[1], Raissa K. Mathura[1], Ben Shofty[1], Victoria Gates[1], Joshua Adkinson[1], Anusha B. Allawala[2], Adrish Anand[1], Ron Gadot[1], Ricardo Najera[1], Hernan G. Rey[1], Sanjay J. Mathew[3], Kelly Bijanki[1], Garrett Banks[1], Andrew Watrous[1], Eleonora Bartoli[1], Sarah R. Heilbronner[1], Nicole Provenza[1], Wayne K. Goodman[4], Nader Pouratian[4], Benjamin Y. Hayden[1] & Sameer A. Sheth[1]

Research on the neural basis of major depressive disorder suggests that it is fundamentally a disease of cortical disinhibition, where breakdowns of inhibitory neuronal systems lead to diminished emotion regulation and intrusive rumination. Subregions of the prefrontal cortex are thought to be sources of this disinhibition. However, due to limited opportunities for intracranial recordings from humans with major depression, this hypothesis has not been directly tested. Here, we use intracranial recordings from the dorsolateral prefrontal, orbitofrontal, and anterior cingulate cortices from patients with major depression to measure daily fluctuations in self-reported depression symptom severity. Results indicate that directed connectivity within the delta frequency band, which has been linked to cortical inhibition, transiently increases intensity during negative mood. Symptom severity also shifts as connectivity patterns within the left and right prefrontal cortices become imbalanced. Our findings support the overarching hypothesis that depression worsens with prefrontal disinhibition and functional imbalance between hemispheres.

Major depressive disorder (MDD) is perhaps the most prevalent of all mood disorders, labeled by the World Health Organization as the single largest contributor to global disability[1,2]. Although clinicians and researchers have made considerable progress towards treating and understanding MDD, the neural basis of the disorder remains perplexing[3,4]. MDD symptom severity varies across time, but the brain activity associated with these changes has received only modest attention within psychiatry[4–6]. There is evidence that daily measurements of symptom severity can provide insight on temporally dynamic pharmaceutical[6] and neurostimulation effects[7]. Studying the neural basis of MDD while accounting for its temporal dynamics has become more crucial as neuromodulatory therapies are further explored[8–11], and adaptive depression inventories are further developed[12]. Cross-sectional longitudinal work has focused on structural changes to brain structures, highlighting increased brainstem white matter volume as a biomarker for MDD[13]. Others have used neuroimaging to measure functional connectivity between the amygdala and dorsolateral prefrontal cortex (dlPFC), reporting that MDD symptom severity correlated with decreased prefrontal-limbic connectivity over time[14]. Most research in this domain has been longitudinal, following participants

[1]Department of Neurosurgery, Baylor College of Medicine, Houston, TX, USA. [2]Department of Biomedical Engineering, Brown University, Providence, RI, USA. [3]Department of Psychiatry and Behavioral Science, Baylor College of Medicine, Houston, TX, USA. [4]Department of Neurological Surgery, University of Texas: Southwestern, Dallas, TX, USA. ✉e-mail: john.myers@bcm.edu

for several months or years, and they often relied on indirect, non-invasive measurements of neural activity.

Few studies have focused on how the electrophysiological activity underlying mood fluctuations varies across hours or days[4,15]. Sani and colleagues (2018) combined intracranial EEG recordings from the orbitofrontal cortex (OFC), anterior cingulate cortex (ACC), insula, amygdala, and hippocampus with machine learning techniques to decode continuous mood state. Spectral power within the OFC was found to be the most common distinguishing feature of mood shifts, but the study did not focus directly on major depression[15]. Similarly, our previous work (Xiao et al. 2023) reported that MDD symptom severity was correlated with increased low-frequency activity and decreased high-frequency activity in frontotemporal regions. Although these studies have made impressive strides towards understanding the neural basis of fluctuations in human mood, neither study focused on connectivity, despite the fact that MDD is well-established as a brain network/system disorder[16–18]. Therapeutic approaches to MDD can greatly benefit from understanding which changes in connectivity correspond to dynamic shifts in symptom severity.

Widespread dysfunction throughout the limbic system and neocortex is associated with major depression[18–21]. The brain regions comprising the limbic system, including the amygdala, ventral striatum, and ACC, show altered functional connectivity compared to controls[19,21]. Patients with MDD often have hyperconnectivity within the default mode network and hypoconnectivity within the frontoparietal dorsal attention network[18,22,23]. Compared to healthy controls, MDD patients also have hypoconnectivity between the right dlPFC and the right ACC[24]. Although neuroimaging studies can provide only an indirect glimpse at neuronal communication, there is considerable evidence that maladaptive patterns of connectivity are the underlying causes of the intrusive ruminations associated with depression[25–27]. The critical importance of PFC subregions in MDD has become clearer over time[28,29], but it is unknown how electrophysiological communication *between* PFC subregions is related to symptom severity.

Cognitive processes such as attention and emotion regulation are disrupted in MDD[30–33]. Subregions of the PFC play distinct roles in these processes[29,34,35]. The dlPFC is well known for its dual role in executive function and working memory, which facilitates attention control and prevents emotional distractions[32,36–38]. The dlPFC also coactivates with limbic structures, which further implicates the region as important for affective processing[39]. Historically, the OFC is thought to play a causal role in mood and emotion regulation[40–42]. Electrical stimulation to the OFC can cause dose-dependent improvements in mood[43]. In cases of brain injury, patients with OFC lesions have diminished responses to emotionally salient stimuli, poor behavioral adaptation, and an increased likelihood of developing MDD symptoms[44,45]. Compared to healthy controls, the OFC has shown hypoconnectivity with the ACC in MDD patients, but hyperconnectivity with the right dlPFC[46]. During working memory tasks, hypoconnectivity within the frontoparietal network is also characteristic of MDD patients[47]. Across the literature as a whole, activity patterns within the OFC, dlPFC, and ACC have been highlighted as predictive biomarkers for MDD treatment effects[48]. Thus, given the above considerations, we focused on directed connectivity between the OFC, dlPFC, and the ACC in this study.

Much of the research linking brain network connectivity to MDD has used functional magnetic resonance imaging (fMRI) as the sole measure of neural activity[18,24,29,47]. However, drawing causal inferences from fMRI data generates a unique set of challenges[49]. Given the high correlations between blood-oxygen level-dependent (BOLD) signals and gamma oscillations (> 50 Hz), interpreting neuronal connectivity can be problematic[49,50]. The brain is well known to communicate electrochemically[51], and longer-range, even intralaminar, connectivity is more associated with low frequency oscillations (< 15 Hz)[52,53]. Low-frequency oscillations can even be anticorrelated with the BOLD signal[54], which suggests that brain metabolism could *decrease* with widespread cortical synchronization[55]. Notably, at least one study reported that low-frequency oscillations *increased* with the BOLD signal, albeit in anesthetized rats[56]. Aside from the aforementioned link to gamma oscillations, the relationship between the BOLD signal and neural oscillations remains inconsistent[50,57]. Therefore, for the purpose of interpreting our results, we hold previous work relevant to the *electrophysiology* of MDD in higher regard.

Parallel to the neuroimaging work on MDD, several lines of research have focused specifically on the electrophysiological, molecular, and transcriptomic bases of MDD[28,29,58]. There is strong evidence that the cerebral atrophy associated with MDD is linked to stress-induced excitotoxicity and inflammation[59,60]. The prefrontal 'hypoactivation' (compared to healthy controls) observed in neuroimaging studies may be due to excitotoxicity driven by increased intracellular metabolism and oxidative stress[61]. The major inhibitory neurotransmitter system within the brain, gamma aminobutyric acid (GABA), is compromised in MDD[62]. This breakdown of inhibitory control is likely preventing the healthy modulation of excitatory neurotransmission for MDD patients[63]. The two major 'families' of GABAergic neurons, parvalbumin-positive and somatostatin-positive neurons, are differentially linked to delta oscillations (~1–3 Hz)[64,65], and *both* are damaged in MDD[58]. Mouse models suggest that delta power *decreases* when knocking out parvalbumin-positive neurons, but *increases* when knocking out somatostatin-positive neurons[64]. Somatostatin-positive GABAergic neurons innervate neuronal dendrites[66], and they play a crucial role in synaptic input integration[67]. Thus, delta oscillations may be partially driven by the joint influence of parvalbumin- and somatostatin-positive neurons[64,68].

Classical theories on the origins of low frequency extracellular oscillations suggest that delta reflects the summation of enduring after-hyperpolarizations within pyramidal neurons of layer V, rather than synaptic activity per se[69,70]. Although there is heterogeneity within Layer V, a substantial portion of pyramidal cells within are cortical output cells[71,72]. 'Down states' of these pyramidal cells were thought to produce the extracellular delta oscillations observed in electrophysiology[73,74]. Although there remains considerable debate about the meaning of low-frequency oscillations, their precise phase has been causally linked to cognitive performance measures such as reaction time[75], and the rhythmic timing of sensory selection[76]. Delta oscillations have also been linked to many neurological and neuropsychiatric disorders, ranging from sleep disorders[77] to depression[77,78]. Delta is prominent in the frontal cortex[79], and plays an important role in wakeful resting state[56] and sleep[80]. Delta power even increases during both physical pain[81,82] and panic attacks[83], which supports the theory that delta oscillations are linked to interoceptive monitoring as well[84]. These considerations underscore the potential for resting state delta oscillations within the PFC as key biomarkers that signify neuronal communication underlying negative mood and disrupted emotion regulation.

We hypothesized that delta band directed connectivity, measured by Granger causality between PFC subregions, would reveal the directional patterns of activity underlying transient shifts in mood (i.e., higher vs. lower symptom severity). As part of a clinical trial utilizing DBS to alleviate treatment-resistant depression (TRD) (UH3 NS103549), we implanted six patients with intracranial stereo EEG (sEEG) electrodes and recorded neural oscillations within the dlPFC, OFC, and ACC (Fig. 1A). We found that directed connectivity across these PFC subregions increased with symptom severity. Each hemisphere of the PFC also showed distinct patterns of directed connectivity, where (1) strong biases involving connectivity with the left ACC, and (2) increased communication between the OFC and dlPFC in the right hemisphere, were both linked to transient increases in symptom severity. The results of this study provide evidence that the

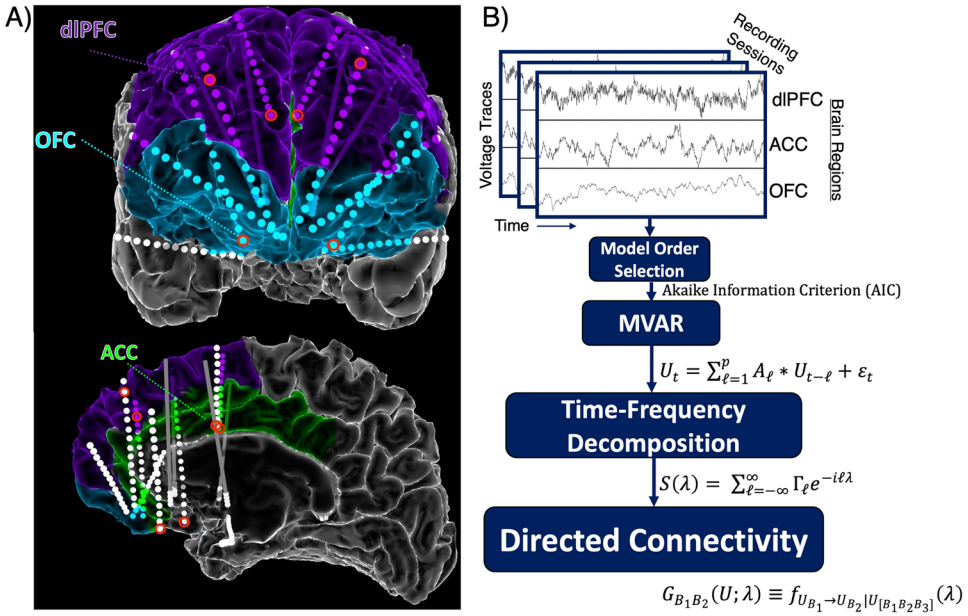

Fig. 1 | Intracranial EEG and directed connectivity. A All participants had intracranial electrodes bilaterally implanted in the prefrontal cortex (PFC). The prefrontal subregions of interest were the dorsolateral prefrontal cortex (dlPFC), the orbitofrontal cortex (OFC), and the anterior cingulate cortex (ACC). Red circles highlight the dlPFC (Area 10/46), OFC (Area 11), and ACC (Area 24/32) contact locations that were selected based on expert ratings of neuroanatomy. For each participant, two contacts per region (one per hemisphere) were selected to compare connectivity within the left vs right PFC. **B** Analysis pipeline shows progression from raw intracranial EEG data to directed connectivity using multivariate autoregressive (MVAR) models (see "Methods"). Brain image generator: multi-modal neuroimaging analysis and visualization tool[151]. OFC orbitofrontal cortex, dlPFC dorsolateral prefrontal cortex, ACC anterior cingulate cortex.

delta oscillations flowing across the PFC increase their intensity with negative shifts in mood.

Results

MDD symptom severity increases with low frequency directed connectivity across the PFC

We recorded iEEG from 6 neurosurgical patients (3 male, 3 female) undergoing deep brain stimulation for TRD. Temporary iEEG electrodes were implanted in the dlPFC (Area 10/46), OFC (Area 11), and ACC (Area 24/32) (Fig. 1). Throughout a ~10-day inpatient monitoring period, we acquired $n = 78$ assessments of symptom severity using the computerized adaptive depression inventory (CAT-DI; 13.0 assessments per patient, std.error = 1.97). CAT-DI scores were approximately normally distributed, ranging from 'normal' to 'severe' (27.0–86.0), and varied similarly across time within subjects (see "Methods").

Resting state iEEG data was recorded as participants focused their eyes on a fixation cross at center-screen on a computer monitor for 5-min duration. For all participants, we selected single grey matter contacts for each PFC subregion based on expert ratings of their anatomic locality within Areas 10/46 (dlPFC), 11 (OFC), and 24/32 (ACC). We measured directed connectivity between PFC subregions via Granger causality (G-causality) (see "Methods"). Our primary goal was to determine how directed connectivity between PFC subregions is correlated with symptom severity.

Directed connectivity from the left OFC to the left dlPFC increased with symptom severity, $z(74) = 3.82$, $p < 0.001$). Similarly, directed connectivity from the left dlPFC to the left OFC was also positively correlated with symptom severity, $z(74) = 3.14$, $p = 0.002$) (Figs. 2 and 3A). The statistically significant interaction between these two pathways (i.e., $OFC_{left} \rightarrow dlPFC_{left}{}^{*}dlPFC_{left} \rightarrow OFC_{left}$) suggests that *bidirectional communication* between the left OFC and left dlPFC is directly linked to transient shifts in mood, $z(74) = -4.97$, $p < 0.001$). Symptom severity was highest when *both* regions exchanged information (Fig. 3A).

Bidirectional communication between the left dlPFC and left ACC also increased with MDD symptom severity, as indicated by the significant $dlPFC_{left} \rightarrow ACC_{left}{}^{*}ACC_{left} \rightarrow dlPFC_{left}$ interaction, $z(74) = -2.32$, $p = 0.020$ (Fig. 3E). Directed connectivity from the left dlPFC to the left ACC was positively correlated with symptom severity, [$dlPFC_{left} \rightarrow ACC_{left}$; $z(74) = 2.66$, $p = 0.008$], as was its counterpart $ACC_{left} \rightarrow dlPFC_{left}$; $z(74) = 2.31$, $p = 0.020$. In the left hemisphere, bidirectional communication between the OFC and ACC was not significantly linked to symptom severity, $z(74) = -1.41$, $p = 0.158$ (Figs. 2A, C and 3C). In the right hemisphere, we observed a marginally significant $OFC_{right} \rightarrow ACC_{right}{}^{*}ACC_{right} \rightarrow OFC_{right}$ interaction, which may indicate that bidirectional communication between the right OFC and right ACC had a more pronounced effect on mood compared to the left hemispheric counterparts, $z(74) = -1.92$, $p = 0.055$. Indeed, directed connectivity from the right OFC to the right ACC significantly increased with symptom severity, [$z(74) = 4.18$, $p < 0.001$], whereas the left hemisphere homologue showed no effect, $z(74) = 1.08$, $p = 0.279$ (Figs. 2 and 3C, D).

The strongest initial distinction between hemispheres was the greater number of significant main effects in the left PFC (4 main effects) vs. the right PFC (1 main effect) (Fig. 2B, C). However, a *t*-test comparing left PFC vs. right PFC effect sizes (i.e., coefficients from generalized estimating equations (GEEs)) showed no significant difference between hemispheres in their relation to symptom severity, $t(5) = 0.92$, $p = 0.402$. In accordance with this quantitative comparison, the pattern of directed connectivity effects was also similar across hemispheres (Fig. 2B, C) and individual participants. All but one participant (5/6; 83.3%) had significant effects within their own time courses (Supplementary Fig. 1). Taken together, these results indicate that PFC subregions increase their communication alongside transient increases in symptom severity. Increased intra-PFC communication may indicate negative shifts in mood and increased attention to emotion regulation.

https://doi.org/10.1038/s41467-025-61487-6

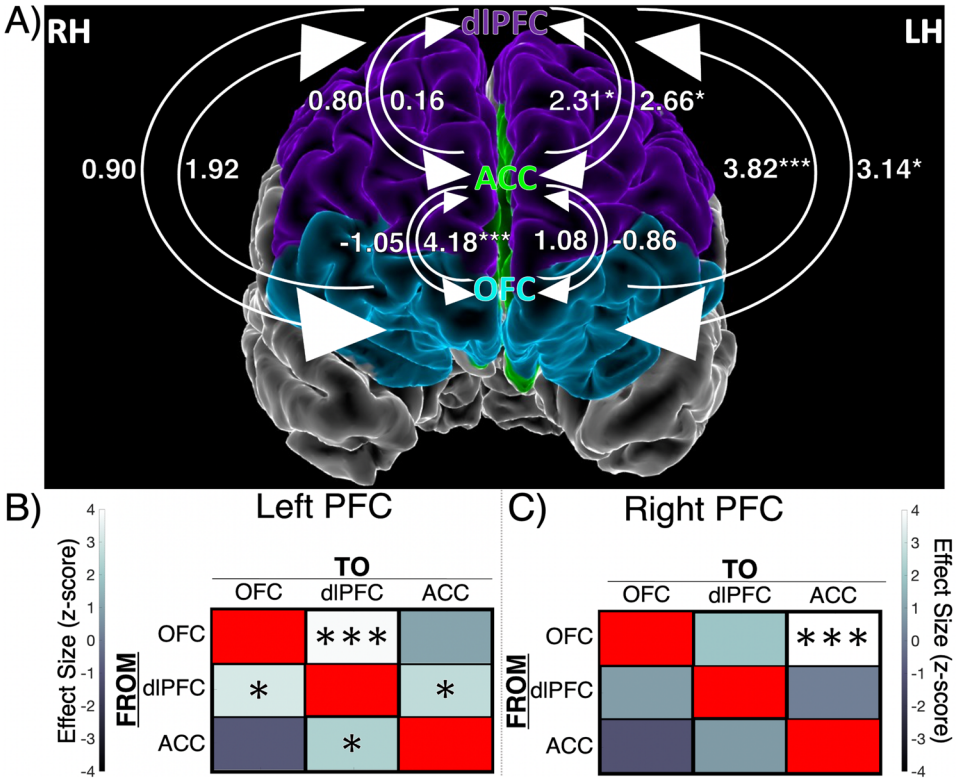

Fig. 2 | Directed connectivity pathways between PFC subregions are linked to symptom severity. A Arrows indicate the direction of connectivity between PFC subregions. The numbers are model coefficients (*z*-scores) from generalized estimating equations (GEEs) showing the relationship between each individual pathway and symptom severity (see "Methods"). Colormaps show graphical representations of the model coefficients in the right PFC (**B**) and left PFC (**C**). Stars indicate statistical significance, $^{*}p < 0.05$, $^{***}p < 0.001$. All results were false-discovery rate (FDR) corrected for multiple comparisons across hemispheres. Brain image generator: multi-modal neuroimaging analysis and visualization tool[151]. OFC orbitofrontal cortex, dlPFC dorsolateral prefrontal cortex, ACC anterior cingulate cortex.

Comparative strength of connectivity within each PFC hemisphere is directly linked to MDD symptom severity

A cursory interpretation of the above analyses might suggest that both hemispheres of the PFC play statistically equivalent roles in depression. However, a series of more direct comparisons between PFC hemispheres revealed stark differences in their relation to symptom severity. We first conducted pairwise comparisons between the left PFC and right PFC homologues (e.g., $ACC_{left} \rightarrow dlPFC_{left}$ *versus* $ACC_{right} \rightarrow dlPFC_{right}$) to determine which hemisphere had stronger inter-regional communication. All communication involving the ACC was higher in the left hemisphere compared to the right hemisphere (Fig. 4). Directed connectivity from the ACC to the dlPFC was significantly higher in the left PFC, $t(77) = 6.20$, $p < 0.001$. Similarly, directed connectivity from the left dlPFC to the ACC was also higher in the left PFC, $t(77) = 4.21$, $p < 0.001$. Directed connectivity from the OFC to the ACC, [$t(77) = 2.52$, $p = 0.014$], as well as from the ACC to the OFC, were also higher in the left hemisphere, $t(77) = 3.06$, $p = 0.005$.

In the right hemisphere, communication was stronger between the OFC and dlPFC. Directed connectivity from the right OFC to the right dlPFC was higher than the left homologue, $t(77) = -2.66$, $p = 0.011$. The reverse was also true, where communication from the dlPFC to the OFC was higher in the right hemisphere, $t(77) = -3.23$, $p = 0.003$ (Fig. 4). These significant differences in connectivity magnitudes across hemispheres inform us about how communication between PFC subregions could be specialized in each hemisphere. Critically, all results reported above were false-discovery rate (FDR) corrected for the multiple comparisons across hemispheres.

Given the observed communicative differences within each PFC hemisphere, we investigated further to determine whether symptom severity was linked to a 'hemispheric differential', which here refers to the arithmetic difference between directed connectivity in the right-minus-left hemisphere (e.g., $ACC_{right} \rightarrow dlPFC_{right} - ACC_{left} \rightarrow dlPFC_{left}$). We subjected these hemispheric differential scores to the same GEE analyses outlined in the "Methods" section to quantify their relationship to depression. Symptom severity increased with the hemispheric differential between the right and left $OFC \rightarrow dlPFC$, revealing a strong bias towards the right hemisphere, $z(74) = 3.69$, $p < 0.001$. Symptom severity was higher when $OFC_{right} \rightarrow dlPFC_{right}$ was greater than $OFC_{left} \rightarrow dlPFC_{left}$ (Fig. 5A). On the other hand, communication between the OFC and ACC showed a left hemisphere bias, where symptom severity decreased when $OFC_{left} \rightarrow ACC_{left}$ was greater than $OFC_{right} \rightarrow ACC_{right}$ (Fig. 5B), $z(74) = -4.96$, $p < 0.001$. Directed connectivity between the left dlPFC and left ACC was also biased towards the left hemisphere, $z(74) = -2.06$, $p = 0.039$. Symptom severity increased when $dlPFC_{left} \rightarrow ACC_{left}$ was greater than $dlPFC_{right} \rightarrow ACC_{right}$.

Collectively, these findings provide clear evidence that the left and right PFC play distinct roles in major depression. The observed differences in directed connectivity magnitudes across hemispheres largely aligned with how the hemispheric differentials correlated with symptom severity. The hemispheric differential results further support the evidence that directed connectivity involving the left ACC is closely linked to symptom severity (Fig. 5B, C). When directed connectivity between the OFC and dlPFC was imbalanced towards the right hemisphere (i.e., right > left), symptom severity was higher (Fig. 5A).

https://doi.org/10.1038/s41467-025-61487-6

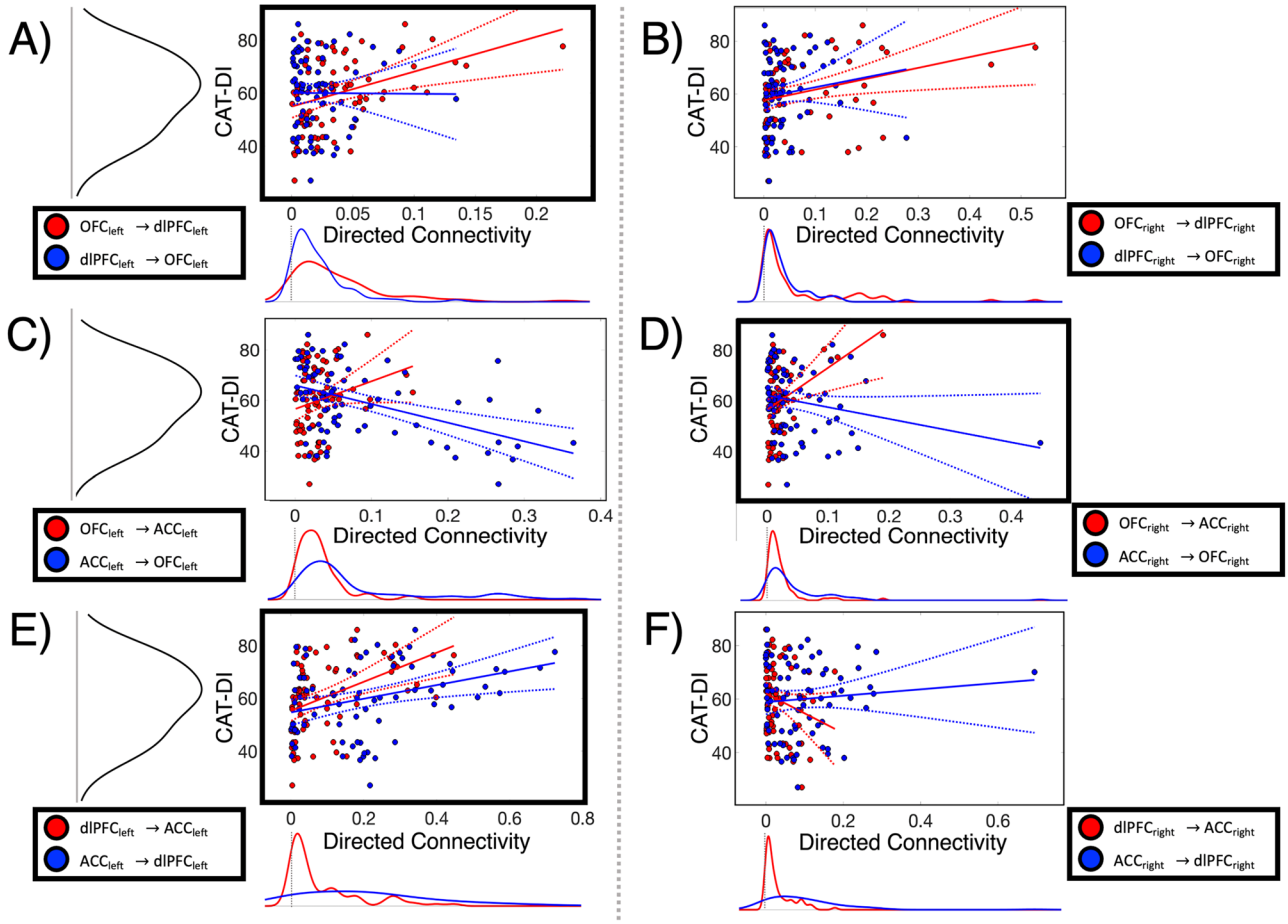

Fig. 3 | A closer look at interactions between PFC subregions and their relation to symptom severity. Scatter plots from GEEs show the relationships between directed connectivity and symptom severity. Depression symptom severity was measured by the computerized adaptive test (CAT-DI: *y*-axes). The x-axes indicate directed connectivity between the subregions labeled in the legends. **A** Symptom severity was positively correlated with directed connectivity between the left OFC and dlPFC ($p < 0.001$). **B** Directed connectivity between the right orbitofrontal cortex (OFC) and dorsolateral prefrontal cortex (dlPFC) were not significantly linked to symptom severity. **C** There were no effects of directed connectivity between the left OFC and anterior cingulate cortex (ACC) on MDD severity ($p > 0.10$). **D** Conversely, directed connectivity from the right OFC to the right ACC was positively correlated with symptom severity (red line: $p < 0.001$). No negative correlation was observed in the reverse direction (blue line: $p = 0.293$). **E** CAT-DI scores positively correlated with directed connectivity from the left dlPFC to the left ACC ($p = 0.008$) and from ACC to dlPFC ($p = 0.020$). There was also a significant interaction between these directed connectivity pathways, where symptom severity increased when information flow between *both* regions increased simultaneously ($p = 0.020$). **F** There were no significant relationships between directed connectivity among the right dlPFC and ACC. These findings expand our understanding on the role of PFC subregions in depression. Regression lines were fit to the data using robust (bi-square) regression for visualization purposes. Dotted lines indicate 95% confidence bounds. Kernel density plots on the *x*- and *y*-axes display probability distributions of the corresponding variables. All results were false-discovery rate (FDR) corrected for multiple comparisons across hemispheres. OFC orbitofrontal cortex, dlPFC dorsolateral prefrontal cortex, ACC anterior cingulate cortex.

Delta spectral power within PFC subregions is linked to MDD symptom severity

Although our primary focus in this work involved prefrontal connectivity, we also measured power spectral density (PSD) within the same delta band (1–3 Hz) to determine how local energy within PFC subregions, instead of communication between them, was related to symptom severity. In the left hemisphere, we observed no effects of delta spectral power on symptom severity (Fig. 6A, C, E). However, in the right hemisphere, spectral power within the OFC [$z(71) = 2.90$, $p = 0.004$] and dlPFC were positively correlated with symptom severity, $z(71) = 2.01$, $p = 0.045$ (Fig. 6B, D). The significant interaction between the spectra of the right OFC and right dlPFC aligns with the effects we found via directed connectivity, where increased delta power in both regions was positively correlated with symptom severity, $z(71) = 2.23$, $p = 0.025$.

We also conducted pairwise *t*-tests to determine which PFC subregions had higher energy across hemispheres. Only the ACC showed significant differences between hemispheres, where the right ACC (mean = 17.99 dB, st.dev = 1.59) had consistently greater spectral power than the left ACC (mean = 17.71 dB, st.dev = 1.52), $t(77) = -5.23$, $p < 0.001$ (Fig. 6E, F). Notably, spectral power within the left OFC was somewhat higher than the right OFC, but the significance did not survive FDR correction, $t(77) = 1.98$, $p = 0.076$. To determine whether there were hemispheric biases in the PSD, we conducted a similar analysis involving the right-minus-left 'power differential'. We observed a right hemispheric bias within the OFC, where symptom severity increased when right OFC delta power was greater than the left OFC, $z(74) = 2.05$, $p = 0.040$ (Fig. 6G). Overall, these PSD effects aligned with those observed for directed connectivity.

Higher frequency directed connectivity is differentially correlated with depression scores

Given the above discoveries regarding the positive correlations between low frequency (delta: 1–3 Hz) directed connectivity and symptom severity, we were motivated to examine directed connectivity at higher frequencies. We analyzed theta (4–7 Hz), alpha

https://doi.org/10.1038/s41467-025-61487-6

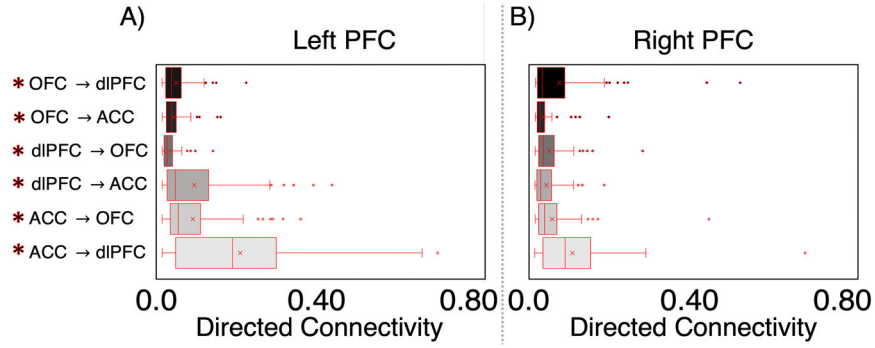

Fig. 4 | Directed connectivity magnitudes across PFC subregions in each hemisphere. Across all participants ($n = 6$), paired two-sided t-tests were conducted between the left PFC and right PFC homologues to determine which hemisphere had stronger inter-regional communication. **A** All communication involving the ACC was higher in the left hemisphere, including directed connectivity from the ACC to the dlPFC ($p < 0.001$), dlPFC to ACC ($p < 0.001$), OFC to ACC ($p = 0.014$), and from the ACC to the OFC ($p = 0.005$). **B** In the right hemisphere, directed connectivity from the orbitofrontal cortex (OFC) to the dlPFC ($p = 0.011$), and from the dlPFC to the OFC was higher ($p = 0.003$). These differences in connectivity magnitudes suggest that communication between PFC subregions is specialized in each hemisphere. All t-test results were false-discovery rate (FDR) corrected for the multiple comparisons across hemispheres. X's within each box show the mean directed connectivity, vertical lines indicate medians. Whiskers mark the minimum and maximum values within 1.5× the upper (Q1) and lower (Q3) interquartile range, and outliers are indicated by single data points beyond this range. *asterisks indicate significant differences between hemispheres ($p < 0.05$). OFC orbitofrontal cortex, dlPFC dorsolateral prefrontal cortex, ACC anterior cingulate cortex.

(8–14 Hz), beta (15–30 Hz), and gamma (31–50 Hz) bands. The magnitudes of directed connectivity followed a typical 1/f pattern, where lower frequencies contain more energy within neural signals (Fig. S4).

Theta directed connectivity from the left ACC to the left OFC, $ACC_{left} \rightarrow OFC_{left}$, was negatively correlated with symptom severity, $z(74) = -2.86$, $p < 0.001$ (Fig. 7A). Both beta ($z(74) = -3.02$, $p = 0.036$) and gamma oscillations ($z(74) = -3.60$, $p < 0.001$) in the reverse direction, $OFC_{left} \rightarrow ACC_{left}$, were negatively correlated with depression scores as well (Fig. 7A). In the right hemisphere, $OFC_{right} \rightarrow ACC_{right}$ theta ($z(74) = 6.40$, $p < 0.001$) and gamma ($z(74) = -3.53$, $p < 0.001$) directed connectivity had opposite correlations with symptom severity. Theta directed connectivity along the $OFC_{right} \rightarrow ACC_{right}$ pathway was positively correlated with depression scores, whereas gamma was negatively correlated (Fig. 7B). Contrarily, theta directed connectivity from the right dlPFC to the right OFC was positively correlated with depression scores, $z(74) = -2.71$, $p = 0.048$. Gamma directed connectivity from the right ACC to the right dlPFC, $ACC_{right} \rightarrow dlPFC_{right}$, was positively correlated with symptom severity, $z(74) = 2.69$, $p = 0.048$. Across all of the above tests, alpha directed connectivity (8–14 Hz) was uncorrelated with symptom severity ($p > 0.50$) (Fig. 7A, B).

We discovered an overarching pattern of results across low vs. high neuronal frequencies by conducting additional analyses comparing the effect sizes (i.e., z-scores) of delta vs. gamma connectivity on CAT-DI scores. Overall, delta (1–3 Hz) connectivity across the PFC was significantly more positively correlated with symptom severity (M = 1.59, SE = 0.49), whereas gamma (31–50 Hz) was more negatively correlated (M = −0.59, SE = 0.56), $t(22) = 2.07$, $p = 0.008$. All results were corrected for false-discovery rates across frequency bands and hemispheres.

Discussion

In this study, we found that transient increases in depression symptom severity were associated with increased directed connectivity between PFC subregions. The unique availability of intracranially measured neural data throughout frontotemporal regions from individuals with severe depression provided by the clinical trial structure allowed us to demonstrate how directed connectivity within the PFC is linked to depression symptoms. Much of the previous work has reported 'hypoactivation' of the PFC as a biomarker of depression[29,61,85,86]. Instead, we found that communication between PFC subregions *increased* with symptom severity. Our results align more closely with the evidence that MDD is related to diminished cortical inhibition[58,87]. Our focus on slow delta oscillations (1–3 Hz) in the PFC provided us with a robust theoretical foundation that facilitated both interpretation and analysis. As previously noted, we focused on delta initially because of its prominence in frontal cortex[88], theorized role in mood disorders[84], and its links to GABAergic inhibition[65,82].

Directed connectivity *from* the OFC to other frontal regions correlated positively with symptom severity. These effects may be related to the increased need for inhibitory control during negative shifts in mood, given that the ACC is involved in emotional response inhibition[89], and the dlPFC is involved in the cognitive control of attention[90]. The OFC's well-known inhibitory control could be compromised in MDD, resulting in ruminations and poor emotion regulation[35,91,92]. Patients with MDD tend to have lower gray matter volume in the OFC and ACC, which may explain this increased 'need' for input from other PFC regions to help stabilize mood[93,94]. The OFC and ACC are functionally connected to mood[46], and we found that delta oscillations between these regions are linked to symptom severity. The crosstalk between PFC subregions may relate to frequent self-appraisals of mood during MDD episodes and diminished control of emotional states[34,95].

There has long been evidence that the left and right hemispheres of the brain serve distinct functions in affective processing and MDD[96,97]. For example, compared to healthy controls, people with MDD often have abnormal perceptual asymmetries during dichotic listening tasks, revealing pathological biases within the brain's right hemisphere[98]. Discoveries such as these led to a heavy emphasis on right-hemispheric activity in research on MDD[99]. In this study, the most distinguishing feature of the right hemisphere was the strong correlation between symptom severity and directed connectivity between the right OFC and right dlPFC (i.e., $OFC_{right} \rightarrow dlPFC_{right}$). This effect aligns with a previous study focused on trait-based differences between MDD patients and healthy controls[46]. By contrast, the most distinguishing feature of the left hemisphere was that all communication pathways involving the left ACC were positively correlated with symptom severity. Imbalanced connectivity between the left and right PFC also seems to contribute to MDD severity, as evidenced by our analyses comparing hemispheres (Fig. 5A, C). Both sets of results from directed connectivity and spectral power analyses align to suggest that communication between and within PFC subregions are distinct in their relationships to major depression. Taken together, these findings support the hypothesis that the left PFC is just as

https://doi.org/10.1038/s41467-025-61487-6

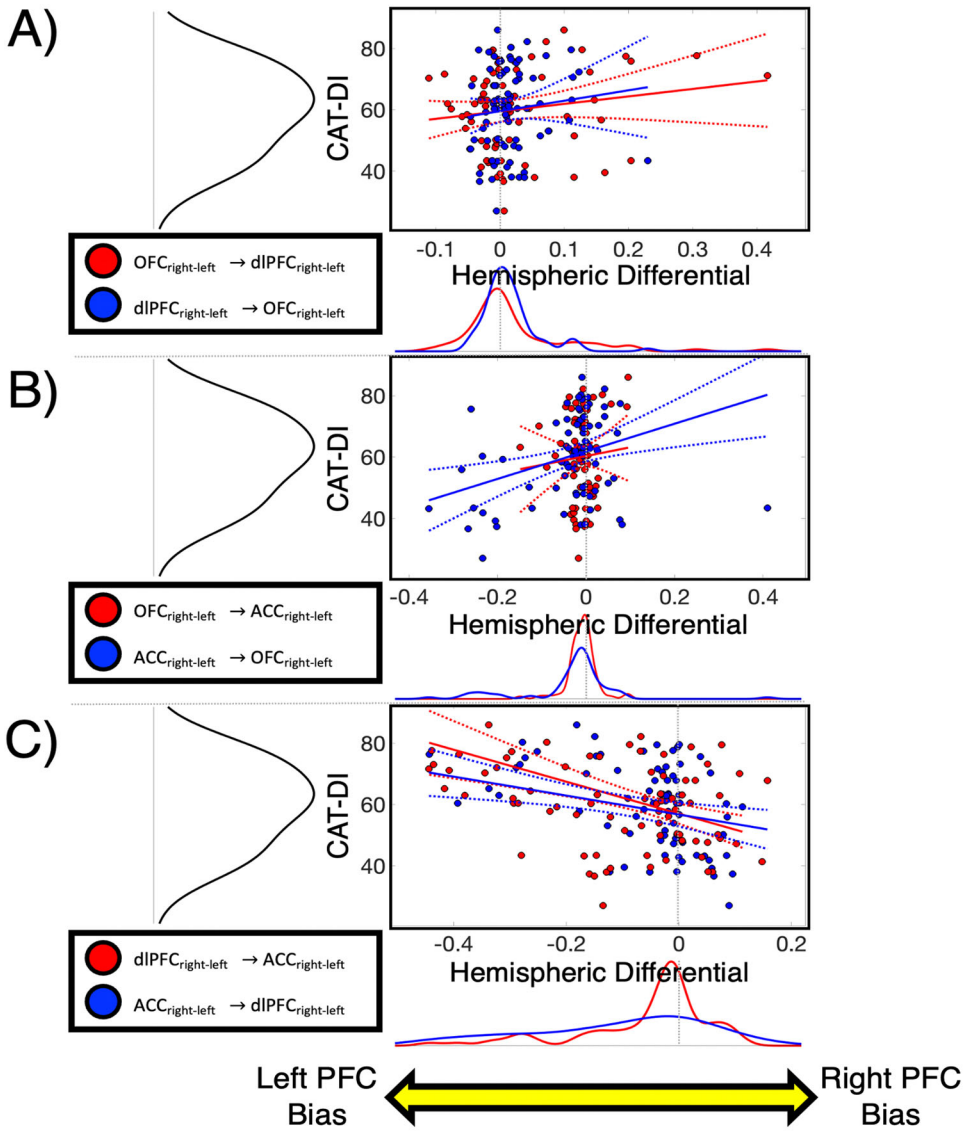

Fig. 5 | Differences between directed connectivity across hemispheres correlate with MDD symptom severity. The 'hemispheric differential' (*x*-axis) refers to the subtractive difference between directed connectivity in the right-minus-left hemisphere. Therefore, positive values on the *x*-axis indicate the strength of right hemisphere bias, and negative values indicate the strength of left hemisphere bias. In order to quantify their relationship to depression, the hemispheric differential scores were subjected to the same GEE analysis structure depicted in Fig. 3. **A** Symptom severity was higher when $OFC_{right} \rightarrow dlPFC_{right}$ was greater than $OFC_{left} \rightarrow dlPFC_{left}$, which indicates a right hemispheric bias ($p < 0.001$). **B** Directed connectivity between the OFC and ACC showed a left hemispheric bias, where symptom severity decreased when $OFC_{left} \rightarrow ACC_{left}$ was higher than $OFC_{right} \rightarrow ACC_{right}$ ($p < 0.001$). **C** Communication between the left dlPFC and ACC was also biased towards the left hemisphere ($p = 0.039$). Symptom severity increased when $dlPFC_{left} \rightarrow ACC_{left}$ was greater than $dlPFC_{right} \rightarrow ACC_{right}$. These results provide clear evidence that the right PFC and left PFC play separate roles in major depression. All results were false-discovery rate (FDR) corrected for multiple comparisons across hemispheres. Dotted lines indicate 95% confidence bounds. OFC orbitofrontal cortex, dlPFC dorsolateral prefrontal cortex, ACC anterior cingulate cortex.

essential for mood regulation as the right PFC[100,101]. The evidence provided here suggests that the two hemispheres play distinct but complementary roles in emotion regulation. Future work may focus on inter-hemispheric PFC interactions across the corpus callosum to elucidate even further. Given that the PFC receives input from several limbic regions[10], the PFC activity observed here was very likely influenced by the amygdala, hippocampus, basal ganglia, and thalamic nuclei as well[31,102]. Future research may employ similar techniques to explore larger scale networks and determine how limbic structures provide information to PFC subregions.

In addition to our findings within low-frequency oscillations (1–3 Hz), we discovered several patterns of directed connectivity within higher frequency bands. The strongest effect revealed that increased theta (4–7 Hz) directed connectivity from the left ACC to the OFC was associated with improved mood (i.e., lower symptom severity). Similarly, increased beta and gamma directed connectivity from the left OFC to the left ACC were negatively correlated with symptom severity as well. These anticorrelated, bidirectional increases of higher frequency oscillations between the left OFC and ACC may be associated with improved mood or emotion regulation[31,34]. In the right hemisphere, theta directed connectivity from the right OFC to the right ACC was positively correlated with symptom severity, whereas gamma was negatively correlated. Theta directed connectivity from the right dlPFC to the right OFC was positively correlated with symptom severity, which aligns with the effect in the delta range, and gamma directed connectivity from the right ACC to the dlPFC also increased with symptom severity. These differential effects across frequency bands evoke the theory of 'oscillatory hierarchy' that

https://doi.org/10.1038/s41467-025-61487-6

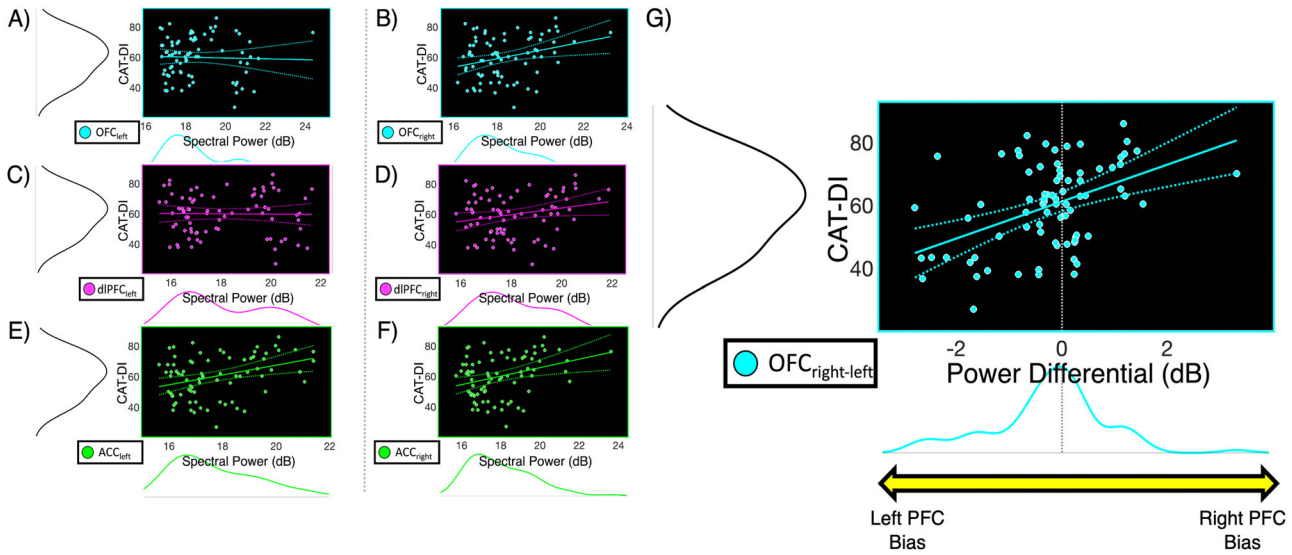

Fig. 6 | Power spectral density in right PFC subregions is linked to symptom severity. A, **C**, **E** In the left hemisphere, we observed no effects of delta spectral power on symptom severity. **B**, **D**, **F** In the right hemisphere, spectral power within the OFC ($p = 0.004$) and dlPFC ($p = 0.045$) were positively correlated with symptom severity. **G** The right-minus-left 'power differential' revealed a right hemispheric bias within the OFC, where symptom severity increased when delta power within the right OFC was greater than the left OFC ($p = 0.040$). All results were computed using GEEs and false-discovery rate (FDR) corrected for multiple comparisons across hemispheres. Dotted lines indicate 95% confidence bounds. OFC orbitofrontal cortex, dlPFC dorsolateral prefrontal cortex, ACC anterior cingulate cortex.

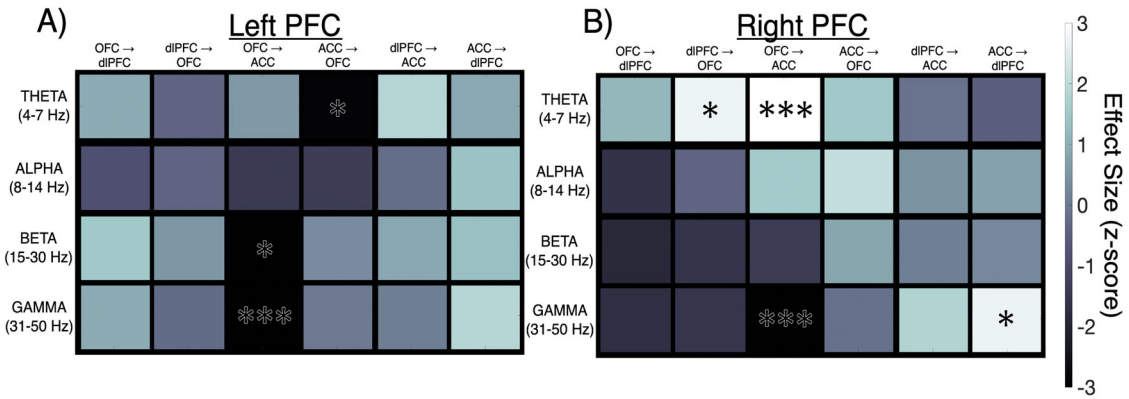

Fig. 7 | MDD symptom severity is differentially correlated with higher frequency directed connectivity. A Theta directed connectivity from the left ACC to the OFC was negatively correlated with symptom severity ($p < 0.001$). Increased beta ($p = 0.036$) and gamma directed connectivity ($p < 0.001$) from the left OFC to the left ACC were also anticorrelated with symptom severity. Increased connectivity via higher frequency oscillations between the left OFC and ACC could be linked to improved mood. **B** In the right hemisphere, theta ($p < 0.001$) and gamma ($p < 0.001$) directed connectivity from the OFC to the ACC had opposite correlations with symptom severity. Theta connectivity was positively correlated with depression scores, whereas gamma was negatively correlated. Theta directed connectivity from the right dlPFC to the OFC was positively correlated with depression scores, ($p = 0.048$). Gamma directed connectivity from the right ACC to the dlPFC was also positively correlated with symptom severity ($p = 0.048$). All results were computed using GEEs and false-discovery rate (FDR) corrected for multiple comparisons across hemispheres. OFC orbitofrontal cortex, dlPFC dorsolateral prefrontal cortex, ACC anterior cingulate cortex.

continues to become more prominent across neuroscience, where neuronal oscillations are both functionally and anatomically organized by frequency[53,103–108]. A recent set of experiments measuring simultaneous low-frequency scalp EEG and high frequency intracranial EEG found increased phase-amplitude coupling between low and high frequency rhythms[109]. Another study using scalp EEG reported prominent phase-amplitude coupling among high and low frequencies in frontal cortex, with whole-brain implications for symptom severity[110]. Future studies using intracranial EEG to study depression should thus be motivated to quantify phase-amplitude coupling across higher and lower frequencies within these prefrontal regions.

Controlled studies using repetitive transcranial magnetic stimulation (rTMS) to target the dlPFC have reported benefits for MDD patients[111,112]. A proposed mechanism for the therapeutic effects of rTMS is connectivity between the dlPFC and the ACC, especially the subgenual cingulate region[113]. Given the bidirectional communication we observed between the left dlPFC and left ACC, combined with their well-known anatomical and functional links[114], our findings were consistent with this proposition. The dlPFC's well-known role in cognitive attention make it a physiologically appropriate candidate when more attention is focused on negative mood[114,115]. Moreover, data from lesion studies suggest that stroke patients with left dlPFC damage are more likely to develop severe MDD symptoms than patients with right dlPFC damage[116]. Although high frequency TMS (~10 Hz) to the left dlPFC is the conventional FDA-approved target for MDD, *bilateral* stimulation may provide greater benefit[112,117].

Recent research using scalp EEG reported that low frequency (delta) functional connectivity was a biomarker for treatment

response, decreasing as mood improved[118]. Higher frequency connectivity, however, was stronger in responders (compared to non-responders) at the beginning of treatment. The results of our study align with these findings but instead show how this low- vs. high-frequency motif exists *within* MDD patients instead of merely between responders and non-responders. We found that low frequency directed connectivity increases with MDD symptom severity, whereas higher-frequency connectivity tends to decrease. Our findings provide deeper anatomical insight into which patterns of neuronal communication could contribute to therapeutic benefit. Increased high frequency (i.e., beta and gamma) projections from the left ACC to the left OFC were anticorrelated with symptom severity. Therefore, discovering which set(s) of neurostimulation parameters reliably increase high-frequency projections from the left ACC to the left OFC (while decreasing low frequency activity elsewhere) would be likely to have the most therapeutic benefit. As we have noted previously (Xiao et al. 2023), the desirability of this pattern of increased high-frequency and decreased low-frequency activity in behavior/symptom-relevant brain regions seems to be a common motif across functional domains. In somatosensory cortex, it predicts faster and more accurate performance with tactile discrimination[119]. In visual cortex, it predicts improved perceptual decision-making[120], and in temporal cortex, it predicts better memory performance[121]. Our results here extend this motif to prefrontal connectivity, where it predicts symptom severity in MDD.

The subgenual cingulate is a well-studied DBS target for severe TRD. This target is considered to be a white matter target at the confluence of important white matter tracts connecting to rostral prefrontal cortex, dorsal cingulate cortex, mesial temporal structures, and brainstem[122]. Alagapan and colleagues (2023) found that neural features from this region derived from a machine learning classifier changed as patients transitioned from 'sick' to 'stable' responses to DBS. Whereas the neural feature is complex, beta power plays a prominent role in the feature. Of note, network-level electrophysiological changes could not be observed due to the singular recording site in the subgenual cingulate. In line with this effect, we found that feedforward beta connectivty from the left OFC to the left ACC increased when symptom severity decreased. Perhaps this discovery is indicative of increased prefrontal regulation of mood. Given the promising results from both invasive neurostimulation of the cingulate and noninvasive stimulation to the PFC, it is clearer now than ever that understanding prefrontal connectivity is integral to treating depression[123,124].

An important question is whether these findings, which describe the neural basis of fluctuations in depressive symptom severity across hours to days, can be relevant to guide neuromodulation therapy. For now, this question is mostly relevant for invasive devices with the capability to record neural activity continuously over long time intervals[124–126]. One application for these data is to serve as inputs for a closed-loop strategy that adjusts stimulation output based on their variations. This strategy may prove useful for DBS for Parkinson's disease[127], in which functional status can fluctuate over hours and stimulation adjustments have rapid effects on symptoms. Neither are true to the same degree for depression. Even though the symptoms of depression may vary over hours as we captured in this study, MDD patients do not vary between depressed and euthymic states with frequency comparable to how patients with Parkinson's disease can fluctuate between dysfunctional "off" states and functional "on" states several times in a day. Stimulation adjustments in Parkinson's often have immediately measurable effects, whereas those for depression may take weeks to months to manifest.

For these reasons, it is likely that closed-loop applications for depression will develop in different ways than they do for disorders with the above temporal and stimulation-response characteristics. Although there is evidence that closed-loop DBS for MDD can be effective in a single patient[128], the authors acknowledged that refined personalization of stimulation parameters would be necessary to increase applicability to larger groups. Our findings with respect to directed connectivity have the potential to aid prognostication to this effect, where stimulation parameters can be modified to promote more clinically beneficial network states. A related possible application of closed-loop DBS would be similar in theme but assessed over longer intervals, designed to make output adjustments with sustained rather than momentary input variations. An alternative promising use of these signals for depression and similar disorders could be as remotely monitorable indicators of clinical status. Such biomarkers are currently unavailable to clinicians and could provide valuable information that the clinician could interpret in the appropriate context. Such "clinician in the loop" strategies have recently been suggested[125]. The most effective of these developing approaches will tailor utilization of these neural biomarkers to the particular features and clinical characteristics of the disorder.

Methods

Participants

Six patients with TRD (3 male; 3 female; avg. age 44.33 y/o) who were implanted with therapeutic DBS leads in the ventral capsule/ventral striatum and sub-callosal cingulate were also implanted with temporary sEEG electrodes in the dlPFC (BA 10/46/47), OFC (BA 11), and ACC (BA 24/32) for neural recordings during a 9-day inpatient monitoring period (see Fig. 1A). These patients were part of an NIH-funded clinical trial via the Brain Research through Advancing Innovative Neurotechnologies (BRAIN) Initiative (UH3 NS103549) and three were the subjects of a previous study about using machine learning to predict symptom severity[4]. All patients provided written and verbal consent to participate in this study, which was approved by the Institutional Review Board at Baylor College of Medicine. All patient-participants were in a depressive episode at the time of the monitoring, as indicated by the clinical evaluation establishing their candidacy for the trial (including DSM diagnostic criteria, clinical impression, MADRS scores, etc.). A table containing the medications, age-of-onset (mean = 19.9 y/o, st.dev = 7.2), and the number of depressive episodes at the time of enrollment (mean = 1.8, st.dev = 1.2) are included in Supplementary Materials (Table S1). No patients were in remission from depression at the time of these recordings.

Intracranial Recordings and Preprocessing

Neural data were recorded while participants were sitting with their eyes focused on a fixation cross at center-screen on a computer monitor (5-min duration). Neural recordings (1–2 per day) most often occurred in the afternoon, with an average start time of 2:04PM ± 4.26 min. All signals were amplified and recorded via sEEG electrodes (2 mm stainless steel contacts with 5 mm spacing; Depthalon, PMT Corporation) at 2 kHz using a Cerebus data acquisition system (Blackrock Microsystems). Signals were bandpass filtered during the recordings at 0.3–500 Hz via Butterworth filter. Single contacts in the dlPFC, OFC, and ACC were selected in each hemisphere by convergence of expert ratings, where authors B.S. and S.H. studied the fused preoperative MRI to postoperative CT images in order to determine whether each contact was within gray matter in the regions of interest (dlPFC, OFC, ACC). Electrode coordinates were acquired via reconstruction in Free-Surfer (https://surfer.nmr.mgh.harvard.edu/). T-tests comparing the absolute values of the x-($p = 0.183$), y- ($p = 0.566$), and z-coordinates ($p = 0.897$) found no significant differences in spatial location. These tests indicate that the anatomic placement of the electrodes were similar across hemispheres and consistent across patients.

All neural data were visually inspected for the presence of recording artifacts by author JX and further examined with automatic rejection based on 3× the standard deviation of spectral power from 1 to 50 Hz by author JM[129]. These procedures were performed in blinded

fashion, i.e., before neural-symptom analyses were performed, to prevent the denoising processes from biasing the results. Channels that were found to be noisy by either method were excluded from further analysis to prevent spread to other channels via re-reference. After data rejection, the following number of clean channels remained for each subject; patient A: 146, patient B: 136, patient C: 136, patient D: 147, patient E: 136, and patient F: 146. As stated above, only 1 contact was chosen for each brain region based on their location within the dlPFC (Area 10/46), OFC (Area 11), and ACC (Area 24/32). The remaining clean channels were balanced across cerebral hemispheres (LH: 48%, RH: 52%). Following bad channel rejection, all remaining channels were notch filtered to attenuate line noise (60 Hz and harmonics) and then re-referenced against adjacent channels via bipolar referencing. Bipolar referencing protects G-causality results from nonlocal sources and noise[130]. Due to the nature of this UH3 clinical trial (NS103549), many of the neural recordings (70.5%) had stimulation experiments conducted within 2.63 h ±18 min of the resting state tasks. Stimulation was delivered to the subgenual cingulate and ventral striatum/ventral capsule via DBS leads. The sEEG contacts within the ACC, dlPFC, and OFC were not stimulated.

MDD symptom severity assessment

We acquired measurements of symptom severity throughout a 9–11 day inpatient monitoring period using the computerized adaptive test for depression inventory (CAT-DI)[131], where higher scores denoted higher symptom severity. Each CAT-DI survey question was adaptively selected based on a patient's previous answers. The CAT-DI can be completed quickly (~12 questions; ~3-min/test), has high test-retest reliability ($r \geq 0.90$), and its scores are highly correlated with other depression inventories that can take much longer for patients to complete[4,131]. The survey data were comprised of 13.0 (std.error = 1.96) CAT-DI assessments from each patient (78 total assessments).

Symptom severity scores ranged from 27.0 to 86.0 (i.e., 'normal' to 'severe'), and a Kolmogorov–Smirnov test indicated an approximately normal distribution ($p = 0.701$) (see Fig. 3). All CAT-DI surveys across subjects contained at least 8 questions, but ranged from 8 to 15 (Fig. S3). The first three survey items of the CAT-DI were strongly correlated with the composite scores ($r_1 = 0.77$, $p_1 < 0.001$; $r_2 = 0.78$, $p_2 < 0.001$; $r_3 = 0.79$, $p_3 < 0.001$). Example questions included, "In the past hour, how much have you been troubled or bothered by psychological or emotional problems?" and "How much were you distressed by feelings of worthlessness?". The seventh item also showed a strong correlation with CAT-DI composite scores ($r_7 = 0.82$, $p_7 < 0.001$), with questions such as "In the past hour, how much of the time have you felt so down in the dumps that nothing could cheer you up?" and "I felt that I could not shake off the blues even with help from my family or friends." A correlation matrix including the first 8 items on the CAT-DI and its composite score is included in Supplementary Materials (Supplementary Fig. 2). The surveys (1–2 per day) were completed prior to the resting state neural recordings, with an average of 24.22 min between the depression surveys and neural recordings. The administration of opioids for post-surgical pain occurred within the first two days of testing. Given the well-known relationship between MDD and physical pain, we evaluated whether the first two days of CAT-DI results were significantly higher than the tests on remaining days. The results of an ANOVA testing the effect of opioid use on CAT-DI across sessions indicated no effect, $F(1, 65) = 0.37$, $p = 0.547$. Throughout the inpatient stay, symptom severity varied similarly across patients, with mean and (standard deviation) of 61.8 (9.18) (Supplementary Fig. 3). The mean score falls within the 'mild' 50–65 range[131].

Directed connectivity modeling

We measured directed connectivity using multivariate vector autoregressive (MVAR) models to quantify information flow across the prefrontal network, comprised of the dlPFC, OFC, and ACC. MVAR models are used to estimate Granger causality (G-causality) in multivariate systems of time series data[132–135]. G-causality measures the extent to which a process, $X_{t=0}$ (i.e., 'X at time zero') can be better predicted by knowing the prior state of process, $Y_{t-\ell}$ (i.e., 'Y at time lag ℓ'), relative to only knowing $X_{t-\ell}$. Therefore, $Y_{t-\ell}$ can only G-cause $X_{t=0}$ if prediction error *decreases* when knowing $Y_{t-\ell}$, compared when knowing only $X_{t-\ell}$. Logically, G-causality is based on the premises that (1) causes occur *before* effects, and that (2) knowledge of causes *reduces* prediction error[136]. We applied this logic to quantify directed connectivity between PFC subregions involved in MDD.

The G-causality measure of interest in this study is the pairwise-conditional spectral causality, $G_{B_1B_2}(U;\lambda) \equiv f_{U_{B_1}} \rightarrow U_{B_2}|U_{[B_1B_2B_3]}(\lambda)$ (1), which computes directed connectivity between two brain regions, $B_1 \rightarrow B_2$, while controlling for the 'universe' of other pairwise relationships, $U_{[B_1B_2B_3]}$[137] (see Fig. 1B). MVAR modeling began with a multivariate matrix, $U_1, U_2, \ldots$ containing all brain regions, B, for all timepoints, t. Each model was constructed as $U_t = \sum_{\ell=1}^{p} A_\ell * U_{t-\ell} + \varepsilon_t$, where p is the model order determined by minimum Akaike Information Criterion from up to 250 milliseconds of data (*model order* ≤ 500)[138]. The regression coefficients, A_ℓ, were estimated using locally weighted regression via the Multivariate Granger Causality (MVGC) toolbox in MATLAB (MathWorks)[137]. All VAR processes were determined to be covariance-stationary by measuring the spectral radius to ensure the functions were invertible within the complex plane (<1.0)[139]. This stationarity test protects G-causality from the slow, unstable dynamics that could diminish their reliability[140]. The MVAR autocovariance sequence, $\Gamma_\ell \equiv \mathrm{cov}(U_t, U_{t-\ell})$, was Fourier transformed to generate the cross-power spectral density (CPSD) of the process, $S(\lambda) = \sum_{\ell=-\infty}^{\infty} \Gamma_\ell e^{-i\ell\lambda}$. The CPSD was then factorized via transfer function, $H(\lambda)$, to $S(\lambda) = H(\lambda) * \sum H(\lambda)^*$, where $H(\lambda)$ is the inverse Fourier transform of the MVAR coefficients. This factorization allows for stable transitions between time and frequency domains, which avoids pitfalls related to separate full vs. reduced model fitting[141,142]. To take advantage of these frequency domain representations, we focused primarily on G-causality within the delta band (1–3 Hz), given its prominence in the frontal cortex[79] (Supplementary Fig. 4).

Power spectral density computations

Power spectral density (PSD) was computed for each PFC contact via wavelet convolution. Each signal, $x(t)$, from a given electrode, was convolved with a Morlet wavelet defined by $\omega(t,f) = Ae^{\frac{-t^2}{2\sigma_t^2}} * e^{i2\pi f_t}$ (2), where A is the normalized amplitude, such that $A = \sigma_t \sqrt{\pi}^{-1/2}$, t is time, f is frequency, and σ_t is wavelet duration[143]. The number of cycles in each wavelet function was 6. All data were analyzed from 1 to 50 Hz in 0.1 Hz intervals, totaling, 491 frequencies. In alignment with the directed connectivity analyses, we focused on the average PSD from 1 to 3 Hz.

Statistical analyses

We used generalized estimating equations (GEEs) to test how resting state *directed connectivity* (*DC*) correlated with symptom severity (*MDD*). The GEEs were constructed as follows. For all subjects $i = 1,\ldots, m$ at times $j = 1, \ldots, n$, $MDD_{ij} = \beta_0 + DC_{R1\rightarrow R2_{i,j}} + DC_{R2\rightarrow R1_{i,j}} + DC_{R1\rightarrow R2_{i,j}} * DC_{R2\rightarrow R1_{i,j}} + e_{i,j}$ (3). The bidirectional communication terms involving both brain regions, *R1↔R2*, were included as well. Given repeated testing of MDD symptom severity, these data are inherently autocorrelated within subjects. Thus, estimating the autocorrelation structure was needed to yield proper GEE parameters. The autocorrelation was estimated by $\alpha_{AR1} = \frac{\sum_{i=1}^{m}\sum_{j=2}^{n_i} z_{i,j} * z_{i,j-1}}{\left(\sum_{i=1}^{m}(n_i-1)-p\right)\varnothing}$ (4), where $z_{i,j}$ and

$z_{i,j-1}$ were the residuals for subject i at time $t_{i,j}$ and time $t_{i,j-1}$, respectively. The dimension of the intercept is given by p and the model-based scaling parameter is $\varnothing$[144,145]. GEEs produce data driven estimates of population-level parameters while accounting for correlations within subjects. These models were computed using 'robust' fitting within the GEEQBOX (MATLAB; MathWorks) to account for potential outliers[144]. The advantages of GEE, in contrast to mixed effect models, can provide more accurate estimates of effects within autocorrelated (i.e., repeated measures) data, with fewer statistical assumptions[145,146]. Each hemisphere of the PFC was analyzed separately to conserve rank for statistical testing and the analysis of interaction effects within hemispheres. There is also evidence that the left and right hemispheres could play distinct roles in MDD[116,147]. In order to test whether symptom severity was linked to differences in directed connectivity between hemispheres, we derived a 'hemispheric differential', which is the subtractive difference between directed connectivity in the right-minus-left hemisphere (e.g., $OFC_{right} \rightarrow dlPFC_{right} - OFC_{left} \rightarrow dlPFC_{left}$). The hemispheric and power differential scores were subjected to the same structure of GEE analyses outlined above. All p-values were false-discovery rate (FDR) corrected to account for multiple comparisons across hemispheres[148]. Although our core objective was to measure correlations between G-causality and symptom severity, we also tested G-causality against theoretical asymptotic null distributions via Geweke's chi-square test in the MVGC toolbox[137,149]. All sessions ($n = 78$) contained statistically significant Granger causality (i.e., greater than zero, $p < 0.05$).

To evaluate the consistency of the electrophysiological measurements, we computed the test-retest reliability of directed connectivity, measured as the intra-class correlations (ICCs) across all directed connectivity variables (6) for each canonical frequency band (5) and hemisphere (2). We also computed ICC across all PSD variables for each brain region (3) and frequency (5). ICC was computed using the Cronbach's alpha method. This method quantifies the consistency of the measurements of neural activity across time and the all brain regions/connections involved. This method is often used in psychometrics to evaluate the consistency of different surveys or ratings[150]. There was substantial consistency across the measures (mean ICC = 0.786). Granger causality was significantly less consistent (mean ICC = 0.63) than the PSD measurements (mean ICC = 0.94), $t(8) = -6.33$, $p = 0.002$, which makes theoretical sense, given that GC is a measure of connectivity in a delayed/lagged temporal space in six directions. PSD, on the other hand, is a simpler measure of the local oscillatory energy within each of the three brain regions. Thus, these differences in consistency align intuitively with the fundamental differences between GC and PSD. We also observed a relationship between ICC and oscillatory frequency. For GC in the left hemisphere, ICC significantly increased with oscillatory frequency ($r = 0.92$, $p = 0.026$). This relationship was visually similar but nonsignificant for right hemisphere GC ($r = 0.76$, $p = 0.136$). PSD variables showed an opposite though nonsignificant trend, where ICC instead decreased with frequency in both the left ($r = -0.26$, $p = 0.678$) and right hemispheres ($r = -0.81$, $p = 0.099$). Although higher frequency GC was more consistent across measurements than low frequency GC (i.e., delta), it was the lower frequency GC which was the strongest indicator of MDD symptom severity (Supplementary Fig. S5). The cluster-correction inherent to generalized estimating equations accounts for variability within-subjects. Notably, these ICC values suggest some degree of collinearity between directed connectivity variables, which is to be expected given that they represent communication between brain regions (often bidirectional). As outlined in the "Statistical Analysis" section below, each pathway (e.g., OFC <-> dlPFC) was analyzed separately to the benefit of interpretability and to prevent over-parametrization.

Reporting summary

Further information on research design is available in the Nature Portfolio Reporting Summary linked to this article.

Data availability

These data are not publicly available to protect the privacy of participants who are involved in the ongoing clinical trial (UH3 NS103549). Contact the corresponding author, John Myers, at john.myers@bcm.edu for reasonable requests and inquiries.

Code availability

The code used in this study is available upon request from the corresponding author J.M. To protect the privacy of participants involved in the ongoing clinical trial (UH3 NS103549) the code is not publicly available.

References

1. WHO. *Depression and Other Common Mental Disorders: Global Health Estimates* (World Health Organization (WHO) **No. WHO/MS**, 2017).
2. Lyus, R., Buamah, C., Pollock, A. M., Cosgrove, L. & Brhlikova, P. Global burden of disease 2017 estimates for major depressive disorder: a critical appraisal of the epidemiological evidence. *JRSM Open* **14**, 20542704231197590 (2023).
3. Mayberg, H. S. et al. Deep brain stimulation for treatment-resistant depression. *Neuron* **45**, 651–660 (2005).
4. Xiao, J. et al. Decoding depression severity from intracranial neural activity. *Biol. Psychiatry* **94**, 445–453 (2023).
5. Fried, E. I. et al. Measuring depression over time… Or not? Lack of unidimensionality and longitudinal measurement invariance in four common rating scales of depression. *Psychol. Assessment.* **28**, 1354 (2016).
6. Johnson, K. M. et al. Evidence to support Montgomery-Asberg depression rating scale administration every 24 hours to assess rapid onset of treatment response. *J. Clin. Psychiatry* **77**, 21987 (2016).
7. Sani, S., Busnello, J., Kochanski, R., Cohen, Y. & Gibbons, R. D. High-frequency measurement of depressive severity in a patient treated for severe treatment-resistant depression with deep-brain stimulation. *Transl. Psychiatry* **7**, e1207–6 (2017).
8. Sheth, S. A. et al. Deep brain stimulation for depression informed by intracranial recordings. *Biol. Psychiatry* https://doi.org/10.1016/j.biopsych.2021.11.007 (2021).
9. Holtzheimer, P. E. et al. Subcallosal cingulate deep brain stimulation for treatment-resistant depression: a multisite, randomised, sham-controlled trial. *Lancet Psychiatry* **4**, 839–849 (2017).
10. Allawala, A. et al. Prefrontal network engagement by deep brain stimulation in limbic hubs. *Front. Hum. Neurosci.* **17**, 1291315 (2024).
11. Riva-Posse, P. et al. A connectomic approach for subcallosal cingulate deep brain stimulation surgery: prospective targeting in treatment-resistant depression. *Mol. Psychiatry* **23**, 843–849 (2017).
12. Grunebaum, M. F., Mann, J. J., Galfalvy, H. C. & Gibbons, R. D. Computerized-adaptive vs. Traditional ratings of depression and suicidal thoughts: an assay sensitivity pilot study in a Ketamine clinical trial. *Front. Psychiatry* **12**, 1–7 (2021).
13. Soriano-mas, C. et al. Cross-sectional and longitudinal assessment of structural brain alterations in melancholic depression. *Biol. Psychiatry* **69**, 318–325 (2010).
14. Sacchet, M. D., Tymo, O., Simmons, A. N. & Yang, T. T. Resting-state functional connectivity of the amygdala and longitudinal changes in depression severity in adolescent depression. *J. Affect. Disord.* **207**, 86–94 (2017).

15. Sani, O. G. et al. Mood variations decoded from multi-site intracranial human brain activity. *Nat. Biotechnol.* **36**, 954 (2018).
16. Northoff, G., Wiebking, C., Feinberg, T. & Panksepp, J. The 'resting-state hypothesis' of major depressive disorder-A translational subcortical-cortical framework for a system disorder. *Neurosci. Biobehav. Rev.* **35**, 1929–1945 (2011).
17. Linkenkaer-Hansen, K. et al. Breakdown of long-range temporal correlations in theta oscillations in patients with major depressive disorder. *J. Neurosci.* **25**, 10131–10137 (2005).
18. Kaiser, R. H., Andrews-Hanna, J. R., Wager, T. D. & Pizzagalli, D. A. Large-scale network dysfunction in major depressive disorder: a meta-analysis of resting-state functional connectivity. *JAMA Psychiatry* **72**, 603–611 (2015).
19. Rolls, E. T. et al. Functional connectivity of the anterior cingulate cortex in depression and in health. *Cereb. Cortex* **29**, 3617–3630 (2019).
20. Fingelkurts, A. A. & Fingelkurts, A. A. Altered structure of dynamic electroencephalogram oscillatory pattern in major depression. *Biol. Psychiatry* **77**, 1050–1060 (2015).
21. Drysdale, A. T. et al. Resting-state connectivity biomarkers define neurophysiological subtypes of depression. *Nat. Med.* **23**, 29–38 (2017).
22. Tozzi, L. et al. Personalized brain circuit scores identify clinically distinct biotypes in depression and anxiety. *Nat. Med.* https://doi.org/10.1038/s41591-024-03057-9 (2024).
23. Ferdek, M. A., van Rijn, C. M. & Wyczesany, M. Depressive rumination and the emotional control circuit: an EEG localization and effective connectivity study. *Cogn. Affect. Behav. Neurosci.* **16**, 1099–1113 (2016).
24. Wang, Y., Yang, S., Sun, W., Shi, Y. & Duan, H. Altered functional interaction hub between affective network and cognitive control network in patients with major depressive disorder. *Behav. Brain Res.* **298**, 301–309 (2016).
25. Mogg, K. & Bradley, B. P. Attentional bias in generalized anxiety disorder versus depressive disorder. *Cognit. Ther. Res.* **29**, 29–45 (2005).
26. Wenzlaff, R. M., Wegner, D. M. & Roper, D. W. Depression and mental control: the resurgence of unwanted negative thoughts. *J. Pers. Soc. Psychol.* **55**, 882 (1988).
27. Li, B. J. et al. A brain network model for depression: from symptom understanding to disease intervention. *CNS Neurosci. Ther.* **24**, 1004–1019 (2018).
28. Howard, D. M. et al. Genome-wide meta-analysis of depression identifies 102 independent variants and highlights the importance of the prefrontal brain regions. *Nat. Neurosci.* **22**, 343–352 (2019).
29. Pizzagalli, D. A. & Roberts, A. C. Prefrontal cortex and depression. *Neuropsychopharmacology* **47**, 225–246 (2022).
30. Rolls, E. T., Cheng, W. & Feng, J. The orbitofrontal cortex: reward, emotion and depression. *Brain Commun.* **2**, fcaa196 (2020).
31. Zheng, K. Z. et al. Incapacity to control emotion in major depression may arise from disrupted white matter integrity and OFC-amygdala inhibition. *CNS Neurosci. Ther.* **24**, 1053–1062 (2018).
32. Wang, L. et al. Prefrontal mechanisms for executive control over emotionaldistraction are altered in major depression. *Psychiatry Res. Neuroimaging* **162**, 143–155 (2008).
33. Loeffler, L. A. K. et al. The regulation of positive and negative emotions through instructed causal attributions in lifetime depression – A functional magnetic resonance imaging study. *NeuroImage Clin.* **20**, 1233–1245 (2018).
34. Dixon, M. L., Thiruchselvam, R., Todd, R. & Christoff, K. Emotion and the prefrontal cortex: an integrative review. *Psychol. Bull.* **143**, 1033–1081 (2017).
35. Rudebeck, P. H. & Murray, E. A. The orbitofrontal oracle: cortical mechanisms for the prediction and evaluation of specific behavioral outcomes. *Neuron* **84**, 1143–1156 (2014).
36. Fales, C. L. et al. Altered emotional interference processing in affective and cognitive-control brain circuitry in major depression. *Biol. Psychiatry* **63**, 377–384 (2008).
37. Heller, A. S. et al. Increased prefrontal cortex activity during negative emotion regulation as a predictor of depression symptom severity trajectory over 6 months. *JAMA Psychiatry* **70**, 1181–1189 (2013).
38. Matsuo, K. et al. Prefrontal hyperactivation during working memory task in untreated individuals with major depressive disorder. *Mol. Psychiatry* **12**, 158–166 (2007).
39. Jung, J. Y., Lambon Ralph, M. A. & Jackson, R. L. Subregions of DLPFC display graded yet distinct structural and functional connectivity. *J. Neurosci.* **42**, 3241–3252 (2022).
40. Harlow, J. Passage of an iron rod through the head. *Bost. Med. Surg. J.* **39**, 389–393 (1848).
41. Schoenbaum, G., Setlow, B., Nugent, S. L., Saddoris, M. P. & Gallagher, M. Lesions of orbitofrontal cortex and basolateral amygdala complex disrupt acquisition of odor-guided discriminations and reversals. *Learn. Mem.* **10**, 129–140 (2003).
42. Szczepanski, S. M. & Knight, R. T. Insights into human behavior from lesions to the prefrontal cortex. *Neuron* **83**, 1002–1018 (2014).
43. Rao, V. R. et al. Direct electrical stimulation of lateral orbitofrontal cortex acutely improves mood in individuals with symptoms of depression. *Curr. Biol.* **28**, 3893–3902.e4 (2018).
44. MacFall, J. R., Payne, M. E., Provenzale, J. E. & Krishnan, K. R. R. Medial orbital frontal lesions in late-onset depression. *Biol. Psychiatry* **49**, 803–806 (2001).
45. Drevets, W. C. Orbitofrontal cortex function and structure in depression. *Ann. N. Y. Acad. Sci.* **1121**, 499–527 (2007).
46. Frodl, T. et al. Functional connectivity bias of the orbitofrontal cortex in drug-free patients with major depression. *Biol. Psychiatry* **67**, 161–167 (2010).
47. Vasic, N., Walter, H., Sambataro, F. & Wolf, R. C. Aberrant functional connectivity of dorsolateral prefrontal and cingulate networks in patients with major depression during working memory processing. *Psychol. Med.* **39**, 977–987 (2009).
48. Lai, C. H. Fronto-limbic neuroimaging biomarkers for diagnosis and prediction of treatment responses in major depressive disorder. *Prog. Neuro-Psychopharmacology Biol. Psychiatry* **107**, 110234 (2021).
49. Ramsey, J. D. et al. Six problems for causal inference from fMRI. *Neuroimage* **49**, 1545–1558 (2010).
50. Carmichael, D. W. et al. Measurement of the mapping between intracranial EEG and fMRI recordings in the human brain. *Bioengineering* **11**, 224 (2024).
51. Bucher, E. S. & Wightman, R. M. Electrochemical analysis of neurotransmitters. *Annu. Rev. Anal. Chem.* **8**, 239–261 (2015).
52. Myers, J. C. et al. The spatial reach of neuronal coherence and spike-field coupling across the human neocortex. *J. Neurosci.* **42**, 6285–6294 (2022).
53. Carracedo, L. M. et al. A neocortical delta rhythm facilitates reciprocal interlaminar interactions via nested theta rhythms. *J. Neurosci.* **33**, 10750–10761 (2013).
54. Feige, B. et al. Cortical and subcortical correlates of electroencephalographic alpha rhythm modulation. *J. Neurophysiol.* **93**, 2864–2872 (2005).
55. Pang, J. C. & Robinson, P. A. Neural mechanisms of the EEG alpha-BOLD anticorrelation. *Neuroimage* **181**, 461–470 (2018).
56. Lu, H. et al. Synchronized delta oscillations correlate with the resting-state functional MRI signal. *Proc. Natl. Acad. Sci. USA.* **104**, 18265–18269 (2007).

57. Logothetis, N. K. The underpinnings of the BOLD functional magnetic resonance imaging signal. *J. Neurosci.* **23**, 3963–3971 (2003).
58. Duman, R. S., Sanacora, G. & Krystal, J. H. Altered connectivity in depression: GABA and glutamate neurotransmitter deficits and reversal by novel treatments. *Neuron* **102**, 75–90 (2019).
59. Popoli, M., Yan, Z., McEwen, B. & Sanacora, G. The stressed synapse: the impact of stress and glucocorticoids on glutamate transmission. *Nat Rev Neurosci* **23**, 1–7 (2013).
60. Wray, N. R. et al. Genome-wide association analyses identify 44 risk variants and refine the genetic architecture of major depression. *Nat. Genet.* **50**, 668–681 (2018).
61. Lu, Y. R., Pei, C., Xie, H. & Li, X. Y. Major depressive disorder and prefrontal cortical metabolism: predictions from snRNA-Seq analysis. *SSRN* (2024).
62. Fee, C., Banasr, M. & Sibille, E. Somatostatin-positive gamma-aminobutyric acid interneuron deficits in depression: cortical microcircuit and therapeutic perspectives. *Biol. Psychiatry* **82**, 549–559 (2017).
63. Ghosal, S., Hare, B. D. & Duman, R. S. Prefrontal cortex GABAergic deficits and circuit dysfunction in the pathophysiology and treatment of chronic stress and depression. *Curr. Opin. Behav. Sci.* **14**, 1–8 (2017).
64. Kuki, T. et al. Contribution of parvalbumin and somatostatin-expressing GABAergic neurons to slow oscillations and the balance in beta-gamma oscillations across cortical layers. *Front. Neural Circuits* **9**, 1–12 (2015).
65. Cardin, J. A. Inhibitory interneurons regulate temporal precision and correlations in cortical circuits. *Trends Neurosci.* **41**, 689–700 (2019).
66. London, M. & Häusser, M. Dendritic computation. *Annu. Rev. Neurosci.* **28**, 503–532 (2005).
67. Song, Y. H., Yoon, J. & Lee, S. H. The role of neuropeptide somatostatin in the brain and its application in treating neurological disorders. *Exp. Mol. Med.* **53**, 328–338 (2021).
68. Zielinski, M. R. et al. Somatostatin+/nNOS+ neurons are involved in delta electroencephalogram activity and corticaldependent recognition memory. *Sleep* **42**, 1–16 (2019).
69. Buzsaki, G. Theta oscillations in the hippocampus. *Neuron* **33**, 325–340 (2002).
70. Buzsaki, G. et al. Nucleus basalis and thalamic control of neocortical activity in the freely moving rat. *J. Neurosci.* **8**, 4007–4026 (1988).
71. Jones, E. G. Microcolumns in the cerebral cortex. *Proc. Natl. Acad. Sci. USA.* **97**, 5019–5021 (2000).
72. Brown, S. P. & Hestrin, S. Intracortical circuits of pyramidal neurons reflect their long-range axonal targets. *Nature* **457**, 1133–1136 (2009).
73. Sirota, A. & Buzsáki, G. Interaction between neocortical and hippocampal networks via slow oscillations. *Thalamus Relat. Syst.* **3**, 245–259 (2005).
74. Buzsáki, G., Anastassiou, C. A. & Koch, C. The origin of extracellular fields and currents — EEG, ECoG, LFP and spikes. *Nat. Rev. Neurosci.* **13**, 407–420 (2012).
75. Stefanics, G. et al. Phase entrainment of human delta oscillations can mediate the effects of expectation on reaction speed. *J. Neurosci.* **30**, 13578–13585 (2010).
76. Schroeder, C. E. & Lakatos, P. Low-frequency neuronal oscillations as instruments of sensory selection. *Trends Neurosci.* **32**, 9–18 (2009).
77. Massicotte-Marquez, J. et al. Slow-wave sleep and delta power in rapid eye movement sleep behavior disorder. *Ann. Neurol.* **57**, 277–282 (2005).
78. Nelson, B. D. et al. Time-frequency reward-related delta prospectively predicts the development of adolescent-onset depression. *Biol. Psychiatry Cogn. Neurosci. Neuroimaging* **3**, 41–49 (2018).
79. Harmony, T. The functional significance of delta oscillations in cognitive processing. *Front. Integr. Neurosci.* **7**, 1–10 (2013).
80. Lanquart, J. P., Nardone, P., Hubain, P., Loas, G. & Linkowski, P. The dichotomy between low frequency and delta waves in human sleep: a reappraisal. *J. Neurosci. Methods* **293**, 234–246 (2018).
81. Bromm, B., Meier, W. & Scharein, E. Pre-stimulus/post-stimulus relations in EEG spectra and their modulations by an opioid and an antidepressant. *Electroencephalogr. Clin. Neurophysiol.* **73**, 188–197 (1989).
82. Li, Y. D. et al. High cortical delta power correlates with aggravated allodynia by activating anterior cingulate cortex GABAergic neurons in neuropathic pain mice. *Pain* **161**, 288–299 (2020).
83. Lesser, I. M., Poland, R. E., Holcomb, C. & Rose, D. E. Electroencephalographs study of nighttime panic attacks. *J. Nerv. Ment. Dis.* **173**, 744–746 (1985).
84. Knyazev, G. G. EEG delta oscillations as a correlate of basic homeostatic and motivational processes. *Neurosci. Biobehav. Rev.* **36**, 677–695 (2012).
85. George, M. S., Ketter, T. A. & Post, R. M. Prefrontal cortex dysfunction in clinical depression. *Depression* **2**, 59–72 (1994).
86. Zhong, M. et al. Amygdala hyperactivation and prefrontal hypoactivation in subjects with cognitive vulnerability to depression. *Biol. Psychol.* **88**, 233–242 (2011).
87. Hamilton, J. P., Chen, G., Thomason, M. E., Schwartz, M. E. & Gotlib, I. H. Investigating neural primacy in major depressive disorder: multivariate Granger causality analysis of resting-state fMRI time-series data. *Mol. Psychiatry* **16**, 763 (2011).
88. Kiss, T., Hoffmann, W. E. & Hajós, M. Delta oscillation and short-term plasticity in the rat medial prefrontal cortex: modelling NMDA hypofunction of schizophrenia. *Int. J. Neuropsychopharmacol.* **14**, 29–42 (2011).
89. Albert, J., López-Martín, S., Tapia, M., Montoya, D. & Carretié, L. The role of the anterior cingulate cortex in emotional response inhibition. *Hum. Brain Mapp.* **33**, 2147–2160 (2012).
90. Smith, E. H. et al. Widespread temporal coding of cognitive control in the human prefrontal cortex. *Nat. Neurosci.* 1–11 https://doi.org/10.1038/s41593-019-0494-0 (2019).
91. Balasubramani, P. P. & Hayden, B. Orbitofrontal neuron ensembles contribute to inhibitory control. Preprint at *bioRxiv* https://doi.org/10.1101/452938 (2018).
92. Cooney, R. E., Joormann, J., Eugène, F., Dennis, E. L. & Gotlib, I. H. Neural correlates of rumination in depression. *Cogn. Affect. Behav. Neurosci.* **10**, 470–478 (2010).
93. Yu, S. et al. The orbitofrontal cortex gray matter is associated with the interaction between insomnia and depression. *Front. Psychiatry* **9**, 1–8 (2018).
94. Bijanki, K. R., Hodis, B., Brumm, M. C., Harlynn, E. L. & McCormick, L. M. Hippocampal and left subcallosal anterior cingulate atrophy in psychotic depression. *PLoS ONE* **9**, 1–7 (2014).
95. Golkar, A. et al. Distinct contributions of the dorsolateral prefrontal and orbitofrontal cortex during emotion regulation. *PLoS ONE* **7**, e48107 (2012).
96. Coffey, C. E. Cerebral laterality and emotion: the neurology of depression. *Compr. Psychiatry* **28**, 197–219 (1987).
97. Quigg, M., Broshek, D. K., Heidal-Schiltz, S., Maedgen, J. W. & Bertram, E. H. Depression in intractable partial epilepsy varies by laterality of focus and surgery. *Epilepsia* **44**, 419–424 (2003).
98. Bruder, G. E., Stewart, J. W. & McGrath, P. J. Right brain, left brain in depressive disorders: clinical and theoretical implications of behavioral, electrophysiological and neuroimaging findings. *Neurosci. Biobehav. Rev.* **78**, 178–191 (2017).

99. Hecht, D. Depression and the hyperactive right-hemisphere. *Neurosci. Res.* **68**, 77–87 (2010).
100. Ochsner, K. N. et al. For better or for worse: neural systems supporting the cognitive down- and up-regulation of negative emotion. *Neuroimage* **23**, 483–499 (2004).
101. Johnstone, T., Van Reekum, C. M., Urry, H. L., Kalin, N. H. & Davidson, R. J. Failure to regulate: counterproductive recruitment of top-down prefrontal-subcortical circuitry in major depression. *J. Neurosci.* **27**, 8877–8884 (2007).
102. Mayberg, H. S. et al. Reciprocal limbic-cortical function and negative mood: converging PET findings in depression and normal sadness. *Am. J. Psychiatry* **156**, 675–682 (1999).
103. Lakatos, P. et al. An oscillatory hierarchy controlling neuronal excitability and stimulus processing in the auditory cortex an oscillatory hierarchy controlling neuronal excitability and stimulus processing in the auditory cortex. *J. Neurophysiol.* **94**, 1904–1911 (2005).
104. Helfrich, R. F. & Knight, R. T. Oscillatory dynamics of prefrontal cognitive control. *Trends Cogn. Sci.* **20**, 916–930 (2016).
105. Von Stein, A. & Sarnthein, J. Different frequencies for different scales of cortical integration: from local gamma to long range alpha/theta synchronization. *Int. J. Psychophysiol.* **38**, 301–313 (2000).
106. Mahjoory, K., Schoffelen, J. M., Keitel, A. & Gross, J. The frequency gradient of human resting-state brain oscillations follows cortical hierarchies. *Elife* **9**, 1–18 (2020).
107. Das, A. et al. Spontaneous neuronal oscillations in the human insula are hierarchically organized traveling waves. *Elife* **11**, 1–27 (2022).
108. Canolty, R. T., Edwards, E., Dalal, S. S., Soltani, M. & Nagarajan, S. S. High Gamma Power Is Phase-Locked to Theta Oscillations in Human Neocortex. *Science* **1626**, 7–8 (2007).
109. Ye, H., Li, G., Sheng, X. & Zhu, X. Phase-amplitude coupling between low-frequency scalp EEG and high-frequency intracranial EEG during working memory task. *J. Neural. Eng.* **19**, 026043 (2022).
110. Raouf, P., Shalchyan, V. & Rostami, R. Investigation of the impact of cross-frequency coupling on the assessment of depression severity through the analysis of resting state EEG signals. *Biomed. Signal Process. Control* **95**, 106392 (2024).
111. Klein, E. et al. Therapeutic efficacy of right prefrontal slow repetitive transcranial magnetic stimulation in major depression: a double-blind controlled study. *Arch. Gen. Psychiatry* **56**, 315–320 (1999).
112. Daskalakis, Z. J., Levinson, A. J. & Fitzgerald, P. B. Repetitive transcranial magnetic stimulation for major depressive disorder: a review. *Can. J. Psychiatry* **53**, 555–566 (2008).
113. Fox, M. D., Buckner, R. L., White, M. P., Greicius, M. D. & Pascual-Leone, A. Efficacy of transcranial magnetic stimulation targets for depression is related to intrinsic functional connectivity with the subgenual cingulate. *Biol. Psychiatry* **72**, 595–603 (2012).
114. Cieslik, E. C. et al. Is there one DLPFC in cognitive action control? Evidence for heterogeneity from Co-activation-based parcellation. *Cereb. Cortex* **23**, 2677–2689 (2013).
115. Kohn, N. et al. Neural network of cognitive emotion regulation - An ALE meta-analysis and MACM analysis. *Neuroimage* **87**, 345–355 (2014).
116. Grajny, K. et al. Depression symptoms in chronic left hemisphere stroke are related to dorsolateral prefrontal cortex damage. *J. Neuropsychiatry Clin. Neurosci.* **28**, 292–298 (2016).
117. Berlim, M. T., Van Den Eynde, F. & Daskalakis, Z. J. A systematic review and meta-analysis on the efficacy and acceptability of bilateral repetitive transcranial magnetic stimulation (rTMS) for treating major depression. *Psychol. Med.* **43**, 2245–2254 (2013).
118. Huang, S. S. et al. Functional connectivity analysis on electroencephalography signals reveals potential biomarkers for treatment response in major depression. *BMC Psychiatry* **23**, 1–11 (2023).
119. Haegens, S., Händel, B. F. & Jensen, O. Top-down controlled alpha band activity in somatosensory areas determines behavioral performance in a discrimination task. *J. Neurosci.* **31**, 5197–5204 (2011).
120. Womelsdorf, T., Fries, P., Mitra, P. P. & Desimone, R. Gamma-band synchronization in visual cortex predicts speed of change detection. *Nature* **439**, 733–736 (2006).
121. Burke, J. F. et al. Human intracranial high-frequency activity maps episodic memory formation in space and time. *Neuroimage* **85**, 834–843 (2014).
122. Riva-Posse, P. et al. Defining critical white matter pathways mediating successful subcallosal cingulate deep brain stimulation for treatment-resistant depression. *Biol. Psychiatry* **76**, 963–969 (2014).
123. Vergani, F. et al. Anatomic connections of the subgenual cingulate region. *Neurosurgery* **79**, 465–472 (2016).
124. Alagapan, S. et al. Cingulate dynamics track depression recovery with deep brain stimulation. *Nature* **622**, 130–138 (2023).
125. Provenza, N. R. et al. Disruption of neural periodicity predicts clinical response after deep brain stimulation for obsessive-compulsive disorder. *Nat. Med.* **30**, 3004–3014 (2024).
126. Provenza, N. R. et al. Long-term ecological assessment of intracranial electrophysiology synchronized to behavioral markers in obsessive-compulsive disorder. *Nat. Med.* **27**, 2154–2164 (2021).
127. Oehrn, C. R. et al. Chronic adaptive deep brain stimulation versus conventional stimulation in Parkinson's disease: a blinded randomized feasibility trial. *Nat. Med.* **30**, 3345–3356 (2024).
128. Scangos, K. W. et al. Closed-loop neuromodulation in an individual with treatment-resistant depression. *Nat. Med.* **27**, 1696–1700 (2021).
129. Delorme, A. & Makeig, S. EEGLAB: an open source toolbox for analysis of single-trial EEG dynamics including independent component analysis. *J. Neurosci. Methods* **134**, 9–21 (2004).
130. Trongnetrpunya, A. et al. Assessing Granger causality in electrophysiological data: removing the adverse effects of common signals via bipolar derivations. *Front. Syst. Neurosci.* **9**, 1–11 (2016).
131. Gibbons, R. D. et al. Development of a computerized adaptive test for depression. *Am. J. Psychiatry* **69**, 187–194 (2012).
132. Krumin, M. & Shoham, S. Multivariate autoregressive modeling and Granger causality analysis of multiple spike trains. *Comput. Intell. Neurosci.* **2010**, 752428 (2010).
133. Bressler, S. L., Kumar, A. & Singer, I. Brain synchronization and multivariate autoregressive (MVAR) modeling in cognitive neurodynamics. *Front. Syst. Neurosci.* **15**, 1–9 (2022).
134. Barrett, A. B., Barnett, L. & Seth, A. K. Multivariate Granger causality and generalized variance. *Phys. Rev. E - Stat. Nonlinear, Soft Matter Phys.* **81**, 1–28 (2010).
135. Bressler, S. L. & Seth, A. K. Wiener-granger causality: a well established methodology. *Neuroimage* **58**, 323–329 (2011).
136. Granger, C. W. J. Economic processes involving feedback. *Inf. Control* **6**, 28–48 (1963).
137. Barnett, L. & Seth, A. K. The MVGC multivariate Granger causality toolbox: a new approach to Granger-causal inference. *J. Neurosci. Methods* **223**, 50–68 (2014).
138. Akaike, H. A new look at the statistical model identification. *IEEE Trans. Automat. Contr.* **19**, 716–723 (1974).
139. Lütkepohl, H. *New Introduction to Multiple Time Series Analysis* (Springer Science & Business Media, 2005).
140. Friston, K. J. et al. Granger causality revisited. *Neuroimage* **101**, 796–808 (2014).

141. Stokes, P. A. & Purdon, P. L. A study of problems encountered in Granger causality analysis from a neuroscience perspective. *Proc. Natl. Acad. Sci. USA.* **114**, E7063–E7072 (2017).
142. Barnett, L., Barrett, A. B. & Seth, A. K. Misunderstandings regarding the application of Granger causality in neuroscience. *Proc. Natl. Acad. Sci. USA.* **115**, E6676–E6677 (2018).
143. Tallon-Baudry, C., Bertrand, O., Delpuech, C. & Pernier, J. Oscillatory γ-band (30–70 Hz) activity induced by a visual search task in humans. *J. Neurosci.* **17**, 722–734 (1997).
144. Ratcliffe, S. J. & Shults, J. GEEQBOX: a MATLAB toolbox for generalized. *J. Stat. Softw.* **25**, 1–14 (2008).
145. Chaganty, N. R. & Shults, J. On eliminating the asymptotic bias in the quasi-least squares estimate of the correlation parameter. *J. Stat. Plan. Inference* **76**, 145–161 (1999).
146. Gardiner, J. C., Luo, Z. & Roman, L. A. Fixed effects, random effects, and GEE: what are the differences? *Stat. Med.* **28**, 221–239 (2009).
147. Cook, I. A., Hunter, A. M., Abrams, M., Siegman, B. & Leuchter, A. F. Midline and right frontal brain function as a physiologic biomarker of remission in major depression. *Psychiatry Res. - Neuroimaging* **174**, 152–157 (2009).
148. Benjamini, Y. & Hochberg, Y. Controlling the false discovery rate: a practical and powerful approach to multiple testing. *Publi. J. R. Stat. Soc.* **57**, 289–300 (1995). author (s): Yoav Benjamini and Yosef Hochberg Source: Journal of the Royal Statistical Society. Series B (Methodological), Vol. 57, No. 1 (1995).
149. Geweke, J. Measurement of linear dependence and feedback between multiple time series. *J. Am. Stat. Assoc.* **77**, 304–313 (1982).
150. McGraw, K. O. & Wong, S. P. Forming inferences about some intraclass correlation coefficients. *Psychol. Methods* **1**, 30–46 (1996).
151. Felsenstein, O. et al. Multi-modal neuroimaging analysis and visualization tool (MMVT). **1**, 1–27 (2019).

Acknowledgements

This work was supported by the National Institutes of Health (Grant No. UH3 NS103549 [to S.A.S., J.M., J.X., R.M., A.B.A., V.G., J.A., S.J.M., W.G., and N.Po.], Grant No. R01 MH106700 [to S.A.S.], Grant Nos. UH3 NS100549 and R01 MH114854 [to W.K.G.], the McNair Foundation (to S.A.S., N.Pr., S.H., B.H.), and the Cain Foundation (to S.A.S.).

Author contributions

J.M., S.J.M., W.K.G., N.Po., and S.A.S. designed research; J.M., J.X., R.K.M., B.S., V.G., J.A., A.B.A., A.A., R.G., R.N., H.G.R., S.J.M., K.B. G.B., J.M., A.W., E.B., and N.Pr. performed research; J.M. and J.X. analyzed data; J.M., S.R.H., B.Y.H., and S.A.S. wrote the paper.

Competing interests

Dr. Sheth has received consultant fees or research support from Boston Scientific, Zimmer Biomet, Koh Young, Neuropace, Varian Medical, Sensoria Therapeutics. He is also co-founder of Motif Neurotech. Dr. Pouratian is a consultant for Abbott Laboratories and Sensoria Therapeutics. Dr. Mathew has received consultant fees or research support from Abbott, Almatica Pharma, Biohaven, BioXcel Therapeutics, Boehringer-Ingelheim, Brii Biosciences, Clexio Biosciences, COMPASS Pathways, Delix Therapeutics, Douglas Pharmaceuticals, Engrail Therapeutics, Freedom Biosciences, Liva Nova, Levo Therapeutics, Merck, Motif Neurotech, Neumora, Neurocrine, Perception Neurosciences, Praxis Precision Medicines, Relmada Therapeutics, Sage Therapeutics, Seelos Therapeutics, Signant Health, Sunovion Pharmaceuticals, Xenon Pharmaceuticals, Worldwide Clinical Trials, and XW Pharma. Dr. Goodman receives royalties from Nview, LLC and OCDscales, LLC. The remaining authors declare no competing interests.

Additional information

Supplementary information The online version contains supplementary material available at https://doi.org/10.1038/s41467-025-61487-6.

Correspondence and requests for materials should be addressed to John Myers.

Peer review information *Nature Communications* thanks Alena Damborská, and the other, anonymous, reviewer(s) for their contribution to the peer review of this work. A peer review file is available.